JOURNAL OF GEOPHYSICAL RESEARCH, VOL. 93, NO. B11, PAGES 13,407–13,420, NOVEMBER 10, 1988

Source Process of the Great 1977 Sumba Earthquake

CHRISTOPHER S. LYNNES[1] AND THORNE LAY

Department of Geological Sciences, University of Michigan, Ann Arbor, Michigan

In order to investigate the applicability of the asperity model to intraplate earthquakes we have studied the rupture process of the great 1977 Sumba normal-faulting earthquake (M_w=8.2–8.3), one of the largest earthquakes since 1963. This event has been variously interpreted as a plate detachment event (i.e., rupture through the entire lithosphere) or a shallow plate-bending event. We have analyzed long-period body waves in order to determine the spatiotemporal rupture characteristics, including the depth extent of the rupture area. Visible depth phases in the initial stage of weak radiation beginning about 15 s before the main pulse suggest that the earthquake nucleated near 29 km depth, which corresponds to the maximum depth of the aftershock sequence. The excitation of a strong tsunami implies that rupture extends to the surface, while deconvolutions of long-period *P* waves suggest a relatively shallow (≤ 50 km) maximum depth extent. However, the existence of slip below this depth cannot be ruled out, particularly if it preferentially radiates frequencies below the passband of the body waves used (< 0.02 Hz). For undiffracted phases the source time function of the principal rupture, which initiated 30 km west of the epicenter of the precursor, comprises a dominant, initial short-duration (24 s) triangular pulse followed by several smaller pulses. However, slightly diffracted phases indicate a simple basic (underlying) character for the rupture, consisting of the initial 24-s triangle superimposed on a longer-duration (42–44 s) trapezoid. The absence of observable directivity in the deconvolved source time functions suggests a bilateral rupture mode. Although the body waves do not require a fault length greater than 80 km, the aftershock area and surface wave results of *Zhang and Kanamori* [1988] imply a total length of at least 200 km. The body wave source functions are well modeled by a 200-km-long fault, extending to 30–50 km depth, on which slip nucleates at the center of the fault and has variable displacement along strike. The peak moment release of the deconvolved source functions indicates higher displacement in the hypocentral area than in other areas of the fault. The spatial relationship of the precursor and the main pulse is suggestive of rupture initiating at and propagating along the edge of an asperity prior to the rupture of the asperity itself. The large size of the event may be due to an unusual stress environment arising from strong lateral gradients in seismic interplate coupling along the Java-Timor arc.

INTRODUCTION

The development of a physical model for earthquake occurrence is a fundamental problem in seismology. One fairly recent conceptual framework, the asperity model, has been successful in explaining many of the physical processes involved in great underthrusting earthquakes, such as coseismic displacement heterogeneity, aftershock and foreshock distribution, and rupture nucleation. However, it is uncertain whether the asperity model is appropriate for great intraplate earthquakes, particularly since the causal stresses are enigmatic. Intraplate seismicity is also extremely sporadic, placing a premium on the amount of information gleaned from each earthquake. In an attempt to investigate the applicability of the asperity model to intraplate earthquakes, we have examined in detail the rupture process of the 1977 Sumba earthquake, especially with regard to the distribution of coseismic displacement and the nucleation of the rupture.

The Sumba earthquake, which occurred within the Indian Plate west of Australia (Figure 1), where it subducts along the Java Trench, was the largest normal-faulting earthquake since the 1933 Sanriku (M_w=8.3) event [*Kanamori*, 1971]. Estimates of the seismic moment based on long-period surface waves and free oscillations range from 24 to 43×10^{27} dyn cm (M_w=8.2–8.3) [*Given and Kanamori*, 1980; *Silver and Jordan*, 1983; *Giardini et al.*, 1985]. This event was well recorded by the World-Wide Standard Seismograph Network (WWSSN), providing a rare opportunity to examine in detail the rupture process of a great intraplate event. Also, since it is one of the five largest earthquakes in the world since 1963, a knowledge of its rupture process would add to our general understanding of the source processes of great earthquakes. Currently, such details are best obtained from long-period *P* waves, which provide better spatial and temporal resolution than surface waves and are relatively uncomplicated by propagation effects. In this study we deconvolve source time functions from long-period *P*, diffracted *P*, and *PP* waves to determine the source process of the 1977 Sumba earthquake.

The International Seismological Centre, Edinburgh, (ISC) location of the Sumba epicenter is 11.16°S, 118.41°E, with an origin time of 0608:54.8 UT on August 19, 1977. This location places the earthquake near the axis of the Java Trench (Figure 1). The relocated 1-month aftershock sequence along the trench extends about 130 km eastward and 110 km westward from the epicenter [*Spence*, 1986]; however, the majority of events cluster about 75 km east of the epicenter (Figure 1). *Dziewonski et al.* [1981] and *Fitch et al.* [1981] inverted body waves from some of the largest aftershocks (all of which have m_b<6.0) and found predominantly normal mechanisms and shallow depths (less than 31 km by *Dziewonski et al.* [1981], less than 24 km by *Fitch et al.* [1981]). *Spence* [1986] used joint hypocentral determinations and depth phases to infer a maximum aftershock depth of 28 km. A subsidiary group of aftershocks with strike-slip mechanisms occurred two months after the Sumba earthquake NNW of the epicenter (Figure 1). *Dziewonski et al.* [1981] and *Fitch et al.* [1981] infer these to be in the upper plate, while *Spence* [1986] locates them in the lower plate. A solitary foreshock (m_b=5.8) occurred about 1 hour before the main shock with approximately the same epicenter.

[1]Now at Teledyne Geotech, Alexandria, Virginia.

Paper number 88JB03225.
0148-0227/88/88JB-03225$05.00

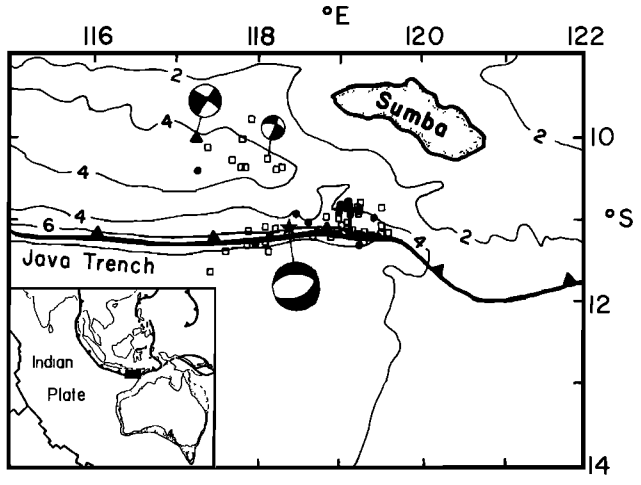

Fig. 1. Bathymetry map of the Java Trench region (contours in kilometers). The epicenter of the main shock is indicated by the star, 1-day aftershocks by the solid circles, and 1-month aftershocks by the open squares. The aftershock epicenters are the relocated values determined by *Spence* [1986]. Focal mechanisms are shown for the main shock [*Given and Kanamori*, 1980] and a representative aftershock in the secondary aftershock area [*Spence*, 1986]. A representative aftershock from a sequence occurring two months later is also shown (triangle) along with its focal mechanism [*Dziewonski et al.*, 1981]. (Inset) Index map of the Indo-Pacific region, with major plate boundaries. The stippled area is the extent of Australian continental crust.

About 150 km to the east of the epicenter and only a few tens of kilometers east of the end of the aftershock area the Java trench is terminated by the apparent resistance of the Australian continental shelf to subduction (Figure 1, inset). The Java arc is similar to the Marianas and Izu-Bonin regions in its lack of great underthrusting events in the historical record, suggesting that the Indian plate is subducting more or less aseismically (i.e., no large or great underthrusting earthquakes). This may be partially attributed to the age (140 Ma) of the oceanic lithosphere being subducted [*Hamilton*, 1979], according to the seismic coupling hypothesis of *Ruff and Kanamori* [1983*b*]. The morphology of the Java subduction zone is also similar to that of the Marianas and Izu-Bonin subduction zones. Downdip of the Java trench the slab dips shallowly to a depth of about 50–100 km, then steepens to a dip of about 80° [*Cardwell and Isacks*, 1978]. The slab extends to a depth of 650 km [*Cardwell and Isacks*, 1978], and *Spence* [1986] has suggested that slab pull is the origin of the tensional stress involved in the 1977 Sumba earthquake sequence and elsewhere along the Java subduction zone in general.

The vertical rupture extent of the Sumba earthquake is problematical. The earthquake produced a large tsunami wave height of 10 m on the island of Sumbawa, which suggests substantial deformation of the ocean bottom and associated fault displacement at very shallow depths. However, the maximum depth extent of the rupture is still uncertain. *Silver and Jordan* [1983] inverted IDA data for the total moment spectrum and inferred a centroid depth of less than 20 km from anomalous spectral peaks that appear when greater source depths are assumed. In a later study employing a similar technique, *Silver et al.* [1986] obtained a centroid of 25 km. *Giardini et al.* [1985] applied the centroid moment tensor (CMT) technique to mantle waves recorded by the GDSN and IDA networks, obtaining a centroid depth of 23 km. On the other hand, *Given and Kanamori* [1980] argue that the relative excitation of fundamental and higher-mode Rayleigh waves from the Sumba earthquake implies a rupture extending to 60–90 km depth. *Zhang and Kanamori* [1985] estimate a depth extent of about 80 km using regional distance Rayleigh waves, overtones, and long-period Love and Rayleigh waves.

As noted above, the aftershocks are well resolved to have depths less than about 30 km. However, the general relationship of mainshock rupture extent to aftershock depths is not straightforward. *Strehlau* [1986] suggests that fault rupture of large continental earthquakes may extend below the deepest aftershocks. Such rupture would probably be smooth and radiate predominantly low frequencies [*Madariaga*, 1983].

Different tectonic interpretations of the 1977 Sumba earthquake have been advanced based on the maximum depth extent. A shallow rupture (< 30 km) would be consistent with a plate-bending event [*Hanks*, 1979], while a rupture extending to greater depths has been taken to imply a plate detachment earthquake [*Stewart*, 1978; *Given and Kanamori*, 1980]. These are fundamentally different models for the deformation of old oceanic lithosphere in subduction zones. However, it should be noted that since the depth of the neutral bending surface is unknown, the depth extent of the 1977 Sumba earthquake alone is insufficient to draw conclusions regarding lithospheric deformation.

In this study we utilize the long-period teleseismic *P* waves to provide additional resolution of the vertical rupture extent as well as of the overall spatial and temporal history of this important earthquake.

BODY WAVE MODELING AND DECONVOLUTIONS

Introduction to Methods

Ruff and Kanamori [1983*a*] develop the theory and technique of time domain deconvolution of a source time function from an observed body wave using a generalized inverse method. This technique has been applied to many large earthquakes to obtain the temporal variations of moment release [e.g., *Ruff and Kanamori*, 1983*a*; *Hartzell and Heaton*, 1985]. Several authors have also been able to resolve spatial variations in the moment release of great earthquakes by directivity analysis of the resulting source functions [e.g., *Beck and Ruff*, 1984, 1985; *Schwartz and Ruff*, 1985]. Another, widely applied procedure is the iterative, multiple-station time domain deconvolution for a finite source model developed by *Kikuchi and Kanamori* [1982] and *Kikuchi and Fukao* [1985]. The latter method also produces characterizations of the spatiotemporal variations of moment release.

In this study we apply both the single-station and multiple-station deconvolution techniques to the 1977 Sumba *P* waves. The single-station method has the advantage of being a linear inversion, which can produce exact fits to the observed seismograms. Also, diffracted seismograms can be deconvolved, although attention must be paid to the effects of diffraction on the results, as discussed below. The multiple-station technique has the advantages of simultaneously fitting all of the observed seismograms with a single source history, and solving directly for the spatial distribution of moment. However, these results must be interpreted with caution because the method locates seismic moment at a particular point on a spatial grid for each iteration, producing an apparently high resolution picture, regardless of the actual spatial resolution inherent in the data set. Also, since absolute amplitude information is utilized,

TABLE 1. Stations Used in Study

Station	Component	Phases	Δ, deg	Φ, deg	Φ_B, deg
AFI	E	P	68	101	263
AKU	Z	P, P_{dif}	118	341	—
ALQ	Z	P_{dif}	133	52	—
ATL	Z	P_{dif}	149	40	—
ATU	E	P_{dif}	100	307	96
BKS	E	P_{dif}	120	53	280
BLA	Z	P_{dif}	149	30	—
COL	E	PP, P_{dif}	102	26	269
COP	E	P_{dif}	108	325	83
DAG	N	PP, P_{dif}	111	350	45
DUG	E	P_{dif}	126	48	288
ESK	E	P_{dif}	117	327	69
FVM	Z	P_{dif}	143	39	—
GDH	Z	P_{dif}	122	357	—
GOL	Z	P_{dif}	132	46	—
IST	E	P_{dif}	97	310	98
KEV	E	P_{dif}	101	339	92
KIP	E	P	88	68	258
KON	E	P_{dif}	109	329	79
LON	Z	P_{dif}	118	43	—
LPA	Z	P_{dif}	134	184	—
LUB	Z	P_{dif}	137	52	—
MAL	Z	P_{dif}	123	306	—
MHI	N	P	73	314	118
MSO	Z	P_{dif}	123	41	—
OGD	Z	P_{dif}	148	19	—
PTO	E	P_{dif}	125	313	72
RAR	Z	P	78	110	—
SCP	Z	P_{dif}	147	23	—
STU	Z	P_{dif}	111	318	—
TUC	Z	P_{dif}	130	57	—
VAL	E	P_{dif}	122	325	64
WES	Z	P_{dif}	148	14	—

Δ is the epicentral distance, Φ is the azimuth to the station, and Φ_B is the back azimuth from the station.

diffracted seismograms are in general not useful in this technique.

Both of the above methods can resolve spatial variations in moment release over length scales of a few tens of kilometers. These methods can also be used to provide some resolution of depth extent, although in very different ways. Since the single-station deconvolution produces an exact fit to each seismogram, the effects of using an incorrect depth are projected entirely into the model space, resulting in distorted source functions. On the other hand, multiple-station deconvolution locates moment release as a function of depth as well as horizontal location; the only assumption that need be made is the depth at which the rupture initiates.

Finally, in interpreting the results of P wave deconvolutions, it is important to remember that the effective bandwidth of long-period P waves is limited, overlapping only slightly the passband of the long-period surface waves and normal modes used in studies yielding average fault properties. The multiple-station deconvolution technique limits the effective passband even more by requiring the use of fairly short period wavelets throughout the inversion in order to match the dominant periods of the seismograms (generally 20–30 s). Thus the macroscopic parameters of the earthquake derived from P waves, such as depth extent, rupture duration, and seismic moment, may differ from those derived from very long period surface waves or normal modes, especially if the earthquake preferentially radiates very long period waves.

Data

Ideally, the P waves used in deconvolutions are azimuthally well distributed and are recorded on vertical component seismographs at distances of 30°–90°. However, for great earthquakes, the vertical component P waves are often off-scale or unreadable, requiring the use of horizontal components and/or diffracted P waves. Horizontal components are frequently noisy, while it is difficult to construct accurate Green's functions for diffracted phases. PP phases in the distance range 90°–123° can also be deconvolved by applying the Hilbert transform to remove the effects of the caustic and free surface reflection [*Lynnes and Ruff*, 1985*b*]. PP phases tend to have slightly higher noise levels than direct P waves, but do yield reliable estimates of seismic moment. In all, four undiffracted P and three PP phases were obtained from WWSSN records of the Sumba earthquake (Table 1).

The large size of the Sumba earthquake did result in many high-quality P recordings at diffracted distances (Table 1). These data provide additional constraints on the rupture process, especially given the limited number of undiffracted observations. Since diffraction is essentially a low-pass filter, it has the effect of suppressing the influence of crustal and water reverberations in the seismograms. This in turn reduces the sensitivity of diffracted seismograms to source and water depth in the deconvolutions. Thus the diffracted seismograms are generally not useful in depth determination; on the other hand, the resultant source functions are more stable with respect to assumed source or water depth. Of course, diffraction also filters the high-frequency components of the source function, thus reducing the spatiotemporal resolution. However, the suppression of higher-frequency components aids in the recovery and identification of the longer-period components of the source process (especially in the time domain). This proves particularly advantageous for the Sumba event because of its unusual moment rate function, as described below.

Model Assumptions

In order to deconvolve source functions from seismograms, the Green's function parameters must first be determined or assumed. Geometric spreading factors for P and PP raypaths for a Jeffreys-Bullen earth model were used, following *Kanamori and Stewart* [1976]. However, since diffraction cannot be described as a frequency-independent geometric spreading effect, the seismic moment estimates obtained from diffracted stations were ignored. Other assumed parameters were a water depth of 4 km, t* (T/Q) of 1.0 for P, pP and sP, t* of 2.0 for PP, pPP and sPP ($T_{PP}/Q \approx 2T_P/Q$), and an average half-space P velocity of 7.6 km/s and density of 3 g/cm^3.

One of the most fundamental input parameters is the focal mechanism. Several authors have published focal mechanisms for the 1977 Sumba event: *Giardini et al.* [1985] obtained a centroid moment tensor solution with a best double couple of strike (ϕ)=264°, dip (δ)=24°, slip (λ)=–73° from long-period surface waves; *Given and Kanamori* [1980] obtained a mechanism of ϕ=270°, δ=45°, λ=–70°, also from long-period waves (Figure 2); and *Spence* [1986] obtained a similar P wave first-motion mechanism of ϕ=279°, δ=45°, λ=–80° (Figure 2). We have chosen the *Given and Kanamori* [1980] surface wave mechanism, since it represents an average mechanism for the full rupture history and is also compatible with Spence's P wave first-motion mechanism and the first motions of the phases used in this study (Figure 2). The *Giardini et al.* [1985] solution

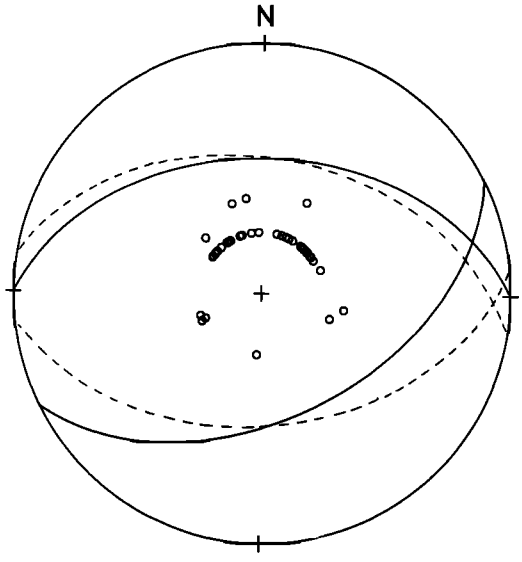

Fig. 2. Lower hemisphere equal-area projection of *Given and Kanamori*'s [1980] mechanism (ϕ=270°, δ=45°, λ=−70°; solid line) and *Spence*'s [1986] *P* wave first-motion mechanism (ϕ=279°, δ=45°, λ=−80°; dashed line). Also shown are the first motions, all dilatations, of the phases used in this study.

violates some of the *P* wave first motions. In any case, most of the phases for which we could recover waveforms leave the focal sphere near the lobe of the *P* radiation pattern, rendering them fairly insensitive to the choice of the focal mechanism.

Depth Determination

Another fundamental parameter that must be specified to construct the Green's function is the depth of the earthquake. As noted earlier, the depth of the Sumba event is problematical and must be treated as a variable. The source process of this event is long enough to obscure depth phases in the observed body waves, as indicated in the representative *P* waveform in Figure 3. However, the main impulsive arrival is preceded by a precursory stage of low energy release beginning about 15 s earlier. (The onset of this precursory radiation actually corresponds to the ISC epicenter and origin time.) Owing to its small size and clear separation from the main pulse, the depth phase *pP* can be identified in some of the seismograms (Figure 4, top). The *P*–*pP* delay time is generally about 6–7 s, corresponding to a depth of about 29 km (Figure 4, bottom) using the upper mantle model PA2 of *Lerner-Lam and Jordan* [1987]. Thus the Sumba earthquake appears to have nucleated with weak radiation near the downdip edge of the subsequent aftershock zone.

In order to determine the location of the onset of the main pulse relative to the hypocenter we measured the differential time between the first arrival and the main pulse on 39 seismograms, including many used in the subsequent deconvolutions. We then applied a master event relocation procedure to the differential times, assuming a half-space velocity of 7.6 km/s. This procedure indicated that the main pulse initiated 2±4 km to the south, 30±3 km to the west, and 28±22 km above the focus of the precursor. The relative origin time is 12±3 s. The relative depth obviously trades off severely with the relative origin time, so the exact depth of nucleation of the main pulse is still uncertain. Nevertheless, it appears that the main pulse did not initiate below 30 km depth.

The waveform complexity of the principal radiation for the Sumba earthquake makes any forward modeling approach impractical for determining the rupture extent, as there are inherent tradeoffs between source function and depth. *Christensen and Ruff* [1985] have examined these tradeoffs by deconvolving finite source synthetic seismograms using Green's functions for point sources at several different depths. They found that deconvolutions performed using source depths below the true rupture extent produce source time functions with a characteristic "ringing." To illustrate this behavior, deconvolutions of a synthetic seismogram computed for a point source 15 km deep are shown in Figure 5. Note that the use of an overestimated depth (40 km) in the deconvolutions produces an excellent fit to the seismogram, but at the expense of an oscillatory source function. Underestimating the depth causes only a moderate broadening of the source function [*Christensen and Ruff*, 1985].

In order to determine the best depth for the purposes of deconvolution, we deconvolved the undiffracted phases, starting at the onset of the main pulse, using Green's functions computed for finite sources extending from 1 km depth to depths of 20, 30, 40, 50, 60, and 70 km (Figure 6), assuming a water depth of 4 km. The most reasonable depth extent to adopt is that which minimizes spurious oscillations (i.e., fulfills a parsimony criterion for the moment rate functions) and produces the most consistent source functions for stations with similar azimuths. This depth experiment should provide some resolution on the depth extent of the 1977 Sumba earthquake, at least in so far as the higher-frequency radiation is concerned.

For all of the seismograms, the shallower depths produce the most stable source functions with the smallest number of oscillations. For instance, the moment rate functions for the greater depth extents at DAG have late oscillations nearly as high as the

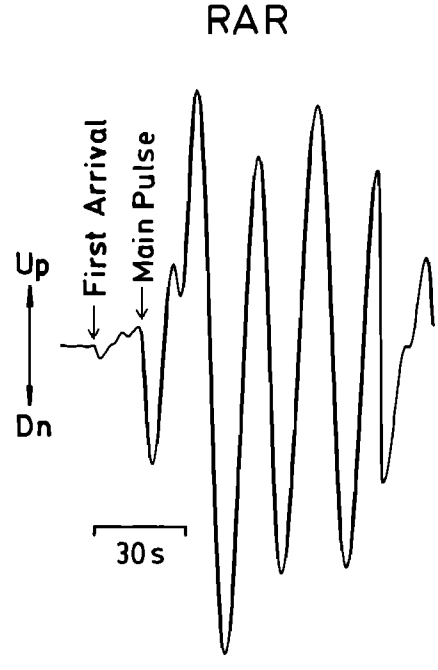

Fig. 3. *P* wave from the vertical component of WWSSN station RAR (Δ=79°, azimuth=110°). The main pulse of the 1977 Sumba earthquake is preceded by a low level of precursory radiation beginning about 15 s earlier, corresponding to the actual origin as reported by ISC.

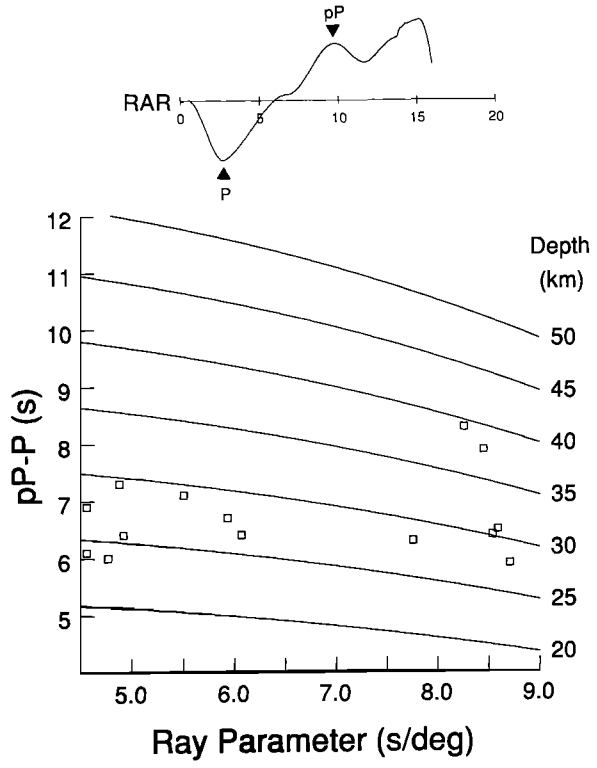

Fig. 4. (Top) Example of "precursor" at RAR showing *P* and *pP* arrivals. (Bottom) Delay times for *pP* phase for several records, plotted as a function of ray parameter on top of theoretical curves for PA2 model of *Lerner-Lam and Jordan* [1987]. The average depth indicated by *pP–P* times is 29 km.

initial pulse, despite the fact that the seismogram itself is completely dominated by an early, long-period, high-amplitude pulse. Similarly, the seismogram at MHI is dominated by a large initial pulse, yet more moment is accumulated in the second half of the source function than in the first half for depth extents greater than 30 km. Unfortunately, the deterioration of the source functions with increasing depth extent is gradual, making an exact determination difficult. However, depth extents of 1–20 km and 1–30 km produce few spurious oscillations at all stations (Figure 6). On the other hand, a depth extent of 1–50 km produces spurious oscillations at several stations (e.g., MHI, KIP, and AKU), and depth extents of 1–60 km and 1–70 km produce source functions that are dominated by later oscillations at all stations. This experiment was repeated assuming water depths of 3, 5, and 6 km, producing very similar results to the above case. Thus the long-period body waves appear to prefer a depth extent of less than about 50 km, with a corresponding centroid near 25 km.

The relatively shallow depth extent obtained from the body waves in this study agrees with the long-period results of *Silver and Jordan* [1983], *Silver et al.* [1986], and *Giardini et al.* [1985], but conflicts with those of *Given and Kanamori* [1980] and *Zhang and Kanamori* [1985]. This conflict may be due to the failure of the WWSSN instruments to adequately recover the very long period components (> 60 s) of the body waves, particularly at the undiffracted stations. However, it should also be noted that the shallow depths given by *Silver and Jordan* [1983], *Silver et al.* [1986], and *Giardini et al.* [1985] were obtained from long-period surface waves. Unfortunately, the limited passband of the body waves precludes a resolution of the differences among the surface wave and normal mode studies.

Single-Station Deconvolution

The final single-station time domain deconvolutions of the main pulse for all *P* wave recordings of the Sumba event were performed with a finite source spanning the depth range 1–30 km. The resulting deconvolutions are shown in order of increasing epicentral distance in Figures 7 and 8. (The deconvolutions of the *PP* phases are plotted according to the distance of the bounce point.) The filtering effects of diffraction around the core at distances greater than 90° are clearly visible. High-frequency features are suppressed, and low-frequency components become more prominent. The Green's functions do not account for the diffraction effects, so the resulting source functions are low-pass filtered versions of the undiffracted source functions.

The source functions deconvolved from the undiffracted phases are dominated by an initial triangular pulse peaking at about 12–14 s and lasting about 24 s. This is followed at many stations by one or two smaller pulses. While it is possible that these later pulses may be due to an incorrect parameterization of water reverberations, perturbations of the source and/or water depth failed to remove them, and the pulses are present at stations at all azimuths, as well as at some diffracted stations. Thus it seems likely that there is some high-frequency source radiation after the initial pulse, which we cannot resolve very well.

However, a fairly simple picture of the overall rupture process is provided by the diffracted phases. These yield source functions comprising the initial triangular pulse superimposed on a longer trapezoidal component lasting about 42–44 s. The longer-duration component is not as apparent in the undiffracted

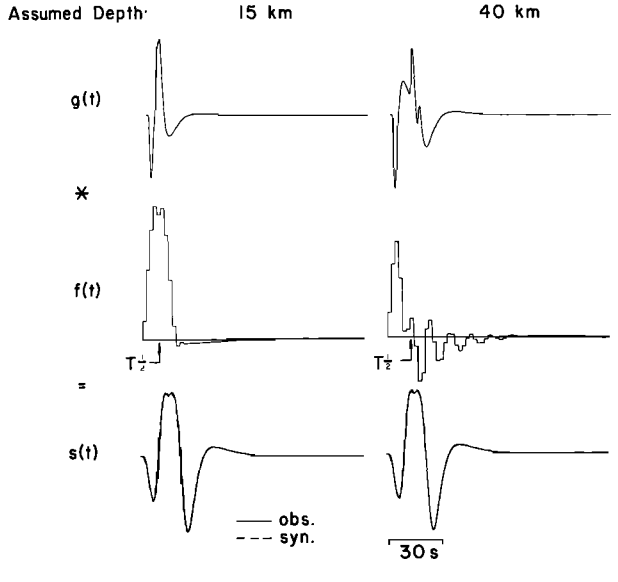

Fig. 5. Example of the effects of overestimated source depth on time domain deconvolution. The top row shows the Green's functions ($g(t)$) computed for the correct depth (15 km) and an incorrect depth (40 km). Although the technique still fits the seismogram very well (bottom row, $s(t)$), the use of the incorrect Green's function produces a "ringing" effect in the source function (middle row, $f(t)$). Using the assumption that the moment rate should be simple and concentrated, we can determine the correct depth.

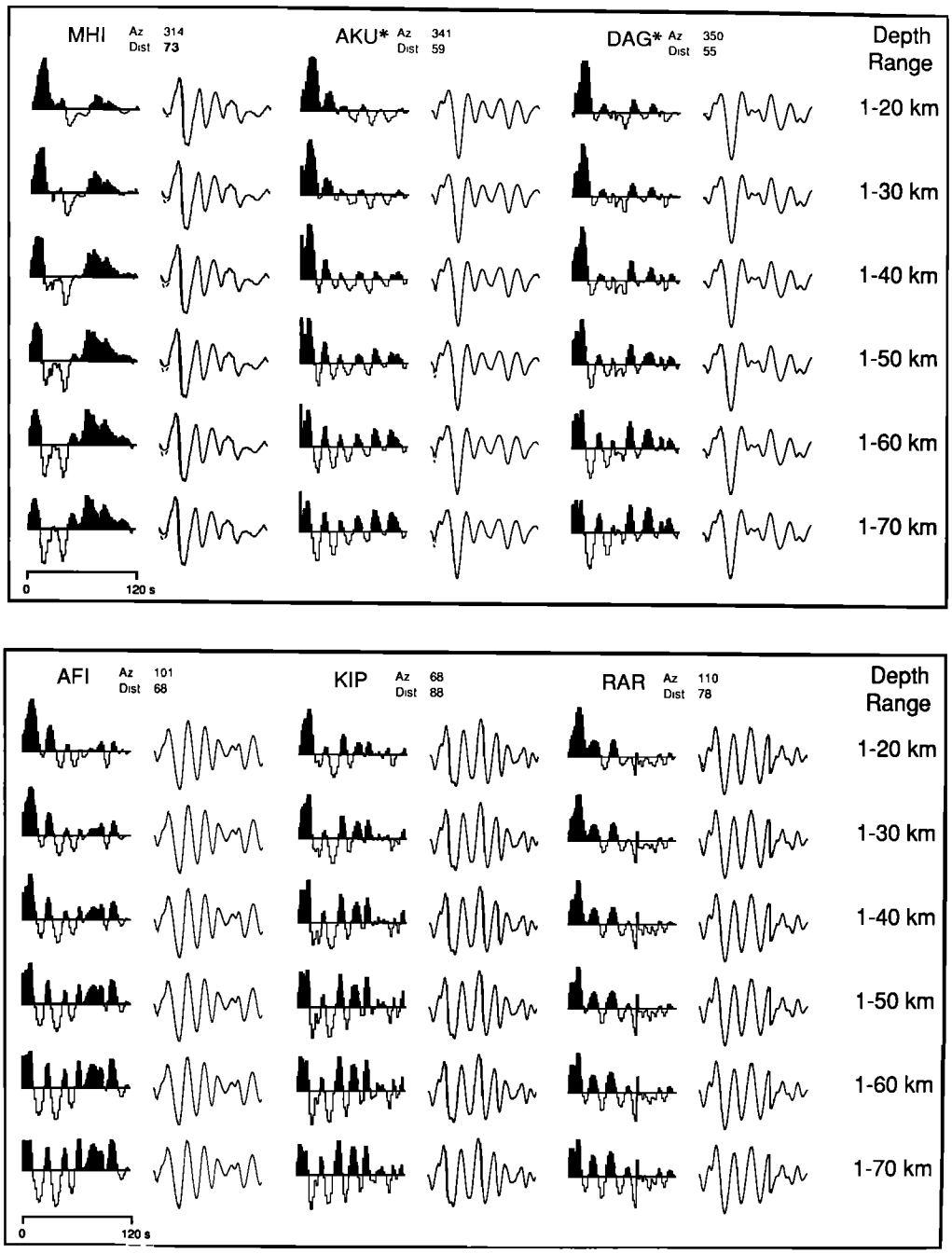

Fig. 6. Deconvolutions of the *P* wave at six undiffracted stations assuming finite sources spanning several different extents. The moment rate functions are shown on the left, while the observed and synthetic (dashed lines) are on the right. The deterioration of the source functions into spurious ringing is gradual, but generally occurs by about 30–50 km.

data because of the very large amplitude high-frequency pulses that arrive on top of it. As the epicentral distance increases, the height ratio of the long-period trapezoid to the initial triangle increases, but the timing and character of the two components change very little, attesting to the stability of the source functions deconvolved from diffracted seismograms. When the duration of this trapezoid is added to the time delay between the precursory energy (corresponding to the actual origin) and the onset of the main pulse (12–15 s), the total duration is 54–59 s. This value is in agreement with the 25-s centroid time (half durations) inferred from normal modes [*Silver et al.*, 1986] and the 67-s rise time (full duration) inferred from long-period surface waves by *Furumoto and Nakanishi* [1983]. However, it is somewhat shorter than the 79 s duration inferred from the long-period surface waves by *Zhang and Kanamori* [1988]. If this is a true discrepancy, it may be explained by the existence of significant very long period radiation outside the body wave passband, possibly from a deeper (> 50 km) extension of the fault.

Source Spectra

The presence of two distinct durations in the diffracted source functions suggests that the source rupture process consists of two components with different characteristic frequencies. We

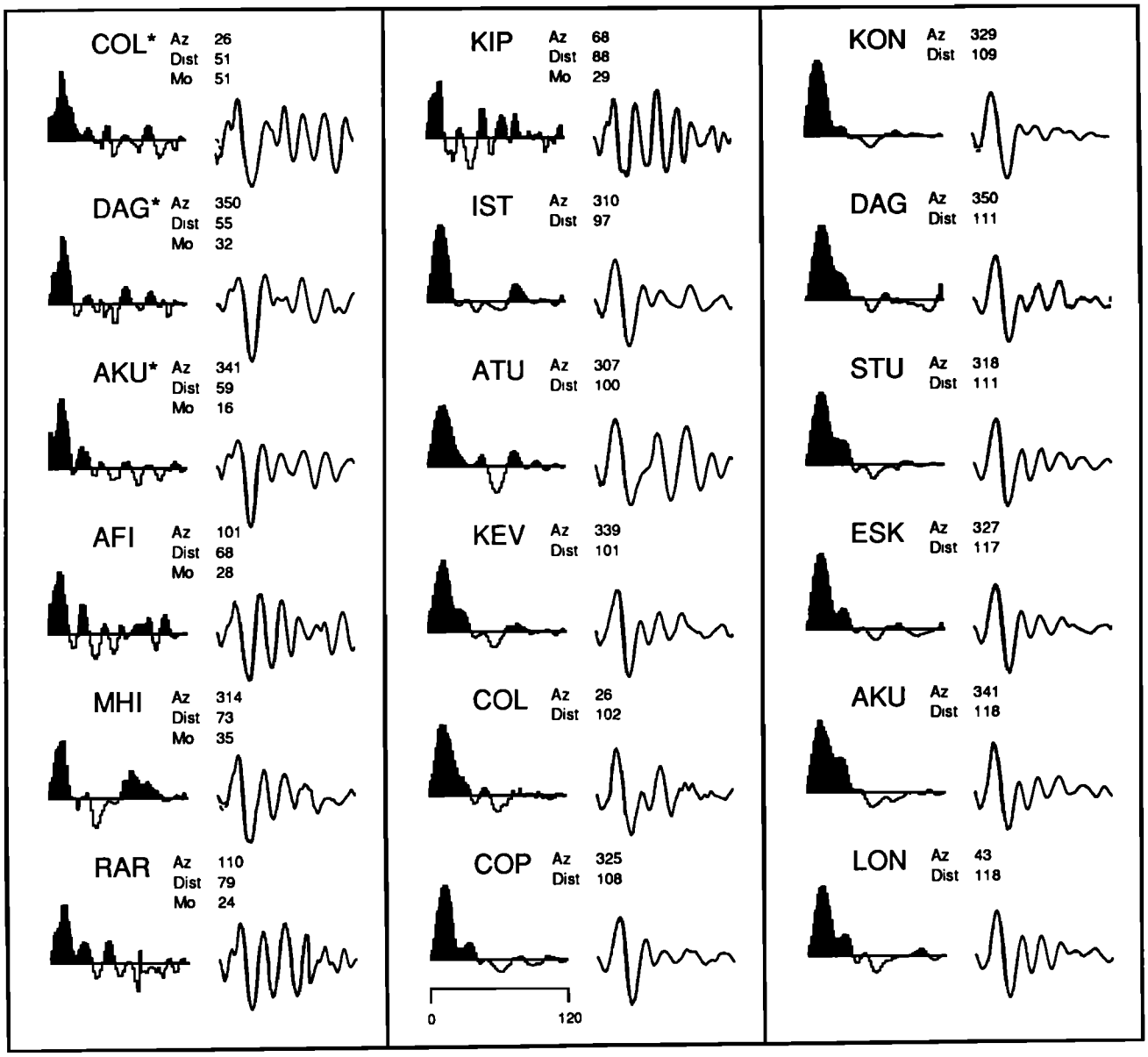

Fig. 7. Single-station time domain deconvolutions, plotted in order of increasing distance. The moment rate functions obtained using a finite source extending from 1 to 30 km depth are shown to the left of the observed (solid) and synthetic (dashed) seismograms. *PP* phases (asterisks) are ordered by the distance of the bounce point. Epicentral distance (Dist) and station azimuth (Az) in degrees are also shown for all stations, and the seismic moment in 10^{27} dyn cm is shown for undiffracted phases.

have transformed the source functions into frequency domain to separate the components more clearly (Figure 9). The source function spectral amplitudes were computed, normalized using the static moment value, and separately stacked for the undiffracted phases ($\Delta<90°$) and the slightly to moderately diffracted phases ($90°<\Delta<110°$). This stacking is valid given the lack of significant azimuthal variations in the source functions.

Both the undiffracted and diffracted source functions exhibit distinct roll-offs at frequencies of about 0.01 and 0.05 Hz, indicating that a long-period component is present in the undiffracted source functions, albeit obscured in the time domain by higher-frequency pulses. The first roll-off corresponds roughly with the 42 to 44-s duration of the trapezoid component visible in the diffracted source functions, and the second roll-off corresponds with the higher-frequency pulses. Comparing the two spectra, the dramatic suppression of the high frequencies by diffraction is apparent, and thus the low-frequency roll-off is much more distinct for the diffracted stations. Nevertheless, the two roll-offs are visible in both spectra and suggest a double corner frequency, which is indicative of two separate characteristic scale lengths operating in the rupture process [*Savage*, 1972].

Seismic Moment

The average seismic moment for the undiffracted phases is $30\pm11 \times 10^{27}$ dyn cm. This is slightly larger than the estimate of 24×10^{27} dyn cm of *Silver and Jordan* [1983], but somewhat smaller than the estimates of 36×10^{27} dyn cm by *Giardini et al.* [1985] and 43×10^{27} dyn cm by *Given and Kanamori*

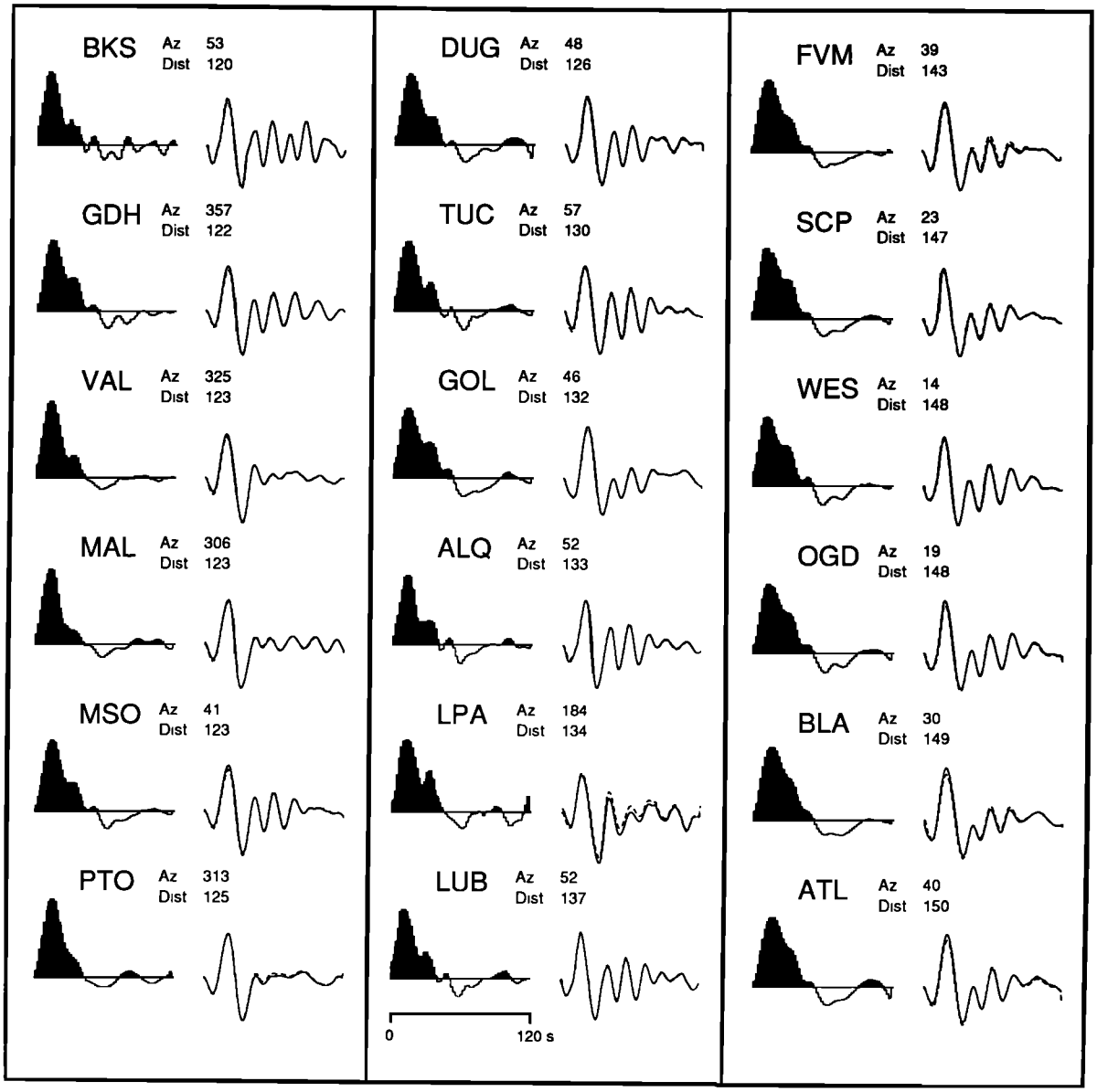

Fig. 8. Same as Figure 7 for diffracted observations in the range 120° to 150°.

[1980]. Both of the latter two estimates, which are based on surface wave excitation, would be reduced if shallower depths were assumed. In contrast, the body wave estimates decrease if greater depth extents are assumed. In other words, there is very little discrepancy between body wave and surface wave estimates using a relatively shallow depth extent, but a rapidly increasing discrepancy as greater depths are assumed. On the other hand, body wave moment estimates from WWSSN seismograms generally tend to underestimate the long-period moment for great earthquakes, occasionally by as much as a factor of 3, because of the limited passband [e.g., *Beck and Ruff*, 1987]. Thus, a failure of the WWSSN instruments to adequately sense very long periods may explain both the depth and seismic moment discrepancies between this study and the surface wave studies of *Given and Kanamori* [1980] and *Giardini et al.* [1985].

Directivity

Resolution of the spatial slip history can often be obtained from systematic azimuthal variations in the timing of features in the moment rate functions [e.g., *Beck and Ruff*, 1984]. The two best candidate features in the Sumba earthquake are the truncation of the higher-frequency triangular pulse occurring at about 14 s and the termination of the long-period pulse at about 42 s. However, the variation of relative delay times for the high-frequency truncation is small (~6 s) and incoherent with respect to station azimuth. This indicates a bilateral and/or short rupture extent. The termination of the long-period trapezoid also varies little, with no coherent azimuthal variation. Although the lack of directivity rules out significant unilateral rupture propagation, it also makes resolution of spatial extent very difficult. The data can be satisfied by either a point source or a fairly long bilateral rupture. However, the aftershock zone is at least

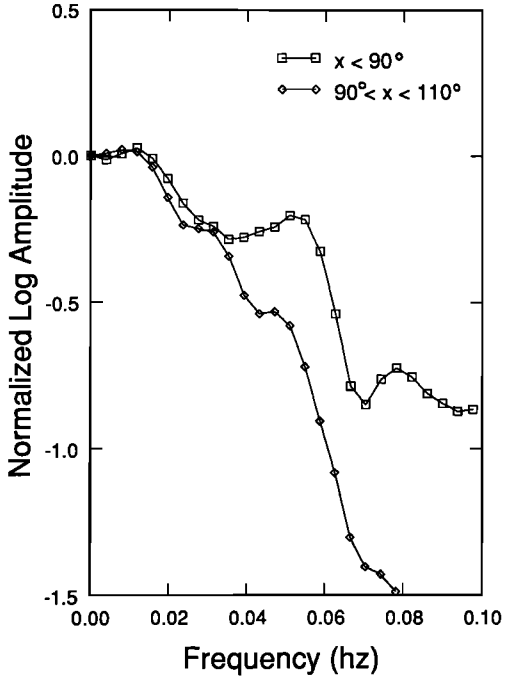

Fig. 9. Source spectra of the single-station deconvolved source time functions in Figure 7, normalized and stacked for undiffracted phases (squares) and for diffracted phases at distances less than 110° (diamonds). Note the double corner frequency apparent for both sets of stations and the suppression of high frequencies by diffraction.

200 km long (Figure 1), which agrees with the model of *Zhang and Kanamori* [1988], who obtained a bilateral rupture of ~200–400 km from an inversion of long-period surface waves, so we will explore a finite fault model with bilateral rupture.

Multiple-Station Deconvolution

In order to further examine the spatial characteristics of the rupture we applied the two-dimensional simultaneous deconvolution technique of *Kikuchi and Fukao* [1985] to the undiffracted body waves of the Sumba event. The source wavelet was constructed using a symmetric trapezoid with a rise time of 5 s and a duration of 7 s, and the same model parameters assumed for the single-station deconvolutions described above. The spatial grid is 11 points and 220 km long along strike, centered on the epicenter of the main pulse. Five points were used in the downdip direction, with depths of 11, 25, 40, 55, and 70 km. The rupture velocity was constrained to be 4 km/s or less. The inversion was performed for five different cases, assuming rupture nucleation at each possible depth. As with the single-station deconvolutions, the low-energy precursor was not included. The results for the southerly dipping nodal plane are shown in Figure 10, but similar results were obtained using the north dipping plane.

Each inversion consisted of 15 iterations, by which time the residual error decreased by about 0.005 from the previous iteration. The convergence was fairly slow, possibly owing to the long-period component in the Sumba source functions, which must be composed of many shorter trapezoids.

The inversion with a hypocenter at the shallowest grid point yielded the smallest residual waveform error (0.26). This shallow nucleation model produces good fits to the waveforms (Figure 11), with much of the error apparently arising from absolute amplitude variations. The horizontal distribution of moment release indicates that most of the moment was released during bilateral rupture near the center, with some bilateral rupture of up to 200 km. However, the distribution of moment along strike is quite unstable with respect to modifications of the model parameters and the exact set of seismograms used. These results are very similar to those obtained with the same technique by *Kikuchi and Fukao* [1987], using a somewhat different seismogram set (and including the initial weak radiation), in that most of the moment is released in bilateral rupture in the vicinity of the onset of the main pulse.

In the downdip direction the proportion of the total moment located by the inversion at the top three grid points is 90% for a nucleation depth of 11 km, 85% for a nucleation depth of 25 km, and 77% for a nucleation depth of 40 km. These three nucleation depths yield essentially equivalent errors, while deeper nucleation points fail to match the data as well. In addition, the top two nucleation points (11 and 25 km) fall within the range indicated by the master event relocation (i.e., no deeper than the precursor depth of 29 km). Thus the multiple-station deconvolution is generally in accord with a relatively shallow depth extent for the fault rupture. This result also agrees with the analysis of *Kikuchi and Fukao* [1987] in the concentration of seismic moment at shallow depths. However, as with the single-station deconvolutions, the simultaneous inversions are intrinsically most sensitive to the dominant shorter periods (~30 s) in the waveforms, so that if there is a small component of long-period body wave radiation from greater depths, it might not be detected at all.

Source Model

The relative simplicity of the 1977 Sumba source functions (Figures 8 and 9) suggests that a simple model can explain most of the data. The model constraints derived above can be summarized as follows: The basic shape of the source function is a triangle superimposed on a longer trapezoid, as indicated in the diffracted seismograms; two distinct length scales are operating in the rupture process; bilateral rupture is indicated by directivity analysis of the single-station deconvolutions and to some degree by the multiple-station analysis; and the depth extent is somewhat limited, probably extending from the surface down to 30–50 km depth. In addition, there may be some smaller, later high-frequency pulses of moment release, as indicated in the undiffracted seismograms. The aftershock distribution also extends to 30 km depth, and about 100–130 km in each direction (east-west) from the epicenter.

One simple model consistent with these observations (except the smaller high-frequency pulses, which we consider to be rather insignificant) would be that of an earthquake nucleating at the center of a homogeneous fault (Figure 12, top) or at the center of the downdip edge (Figure 12, bottom). The moment release rate ($\dot{M}$) is given as (assuming the displacement time is short relative to the rupture time)

$$\dot{M} \approx \mu \dot{A} D$$

where μ is the rigidity, A is the fault area ruptured, and D is the average displacement [*Ruff and Kanamori*, 1983*a*]. Thus the variations in moment rate (i.e., seismic moment accumulated per unit time) for different segments of the fault can be modeled by variations in D or by variations in $\dot{A}$ resulting from changes in the rupture velocity or shape of the rupture front. For instance, if the rupture spreads radially at the beginning with uniform D, a steep rise in the source function will result (Figure 12), with a peak moment release of $\mu(\pi W v_r)D$, where W is the fault width

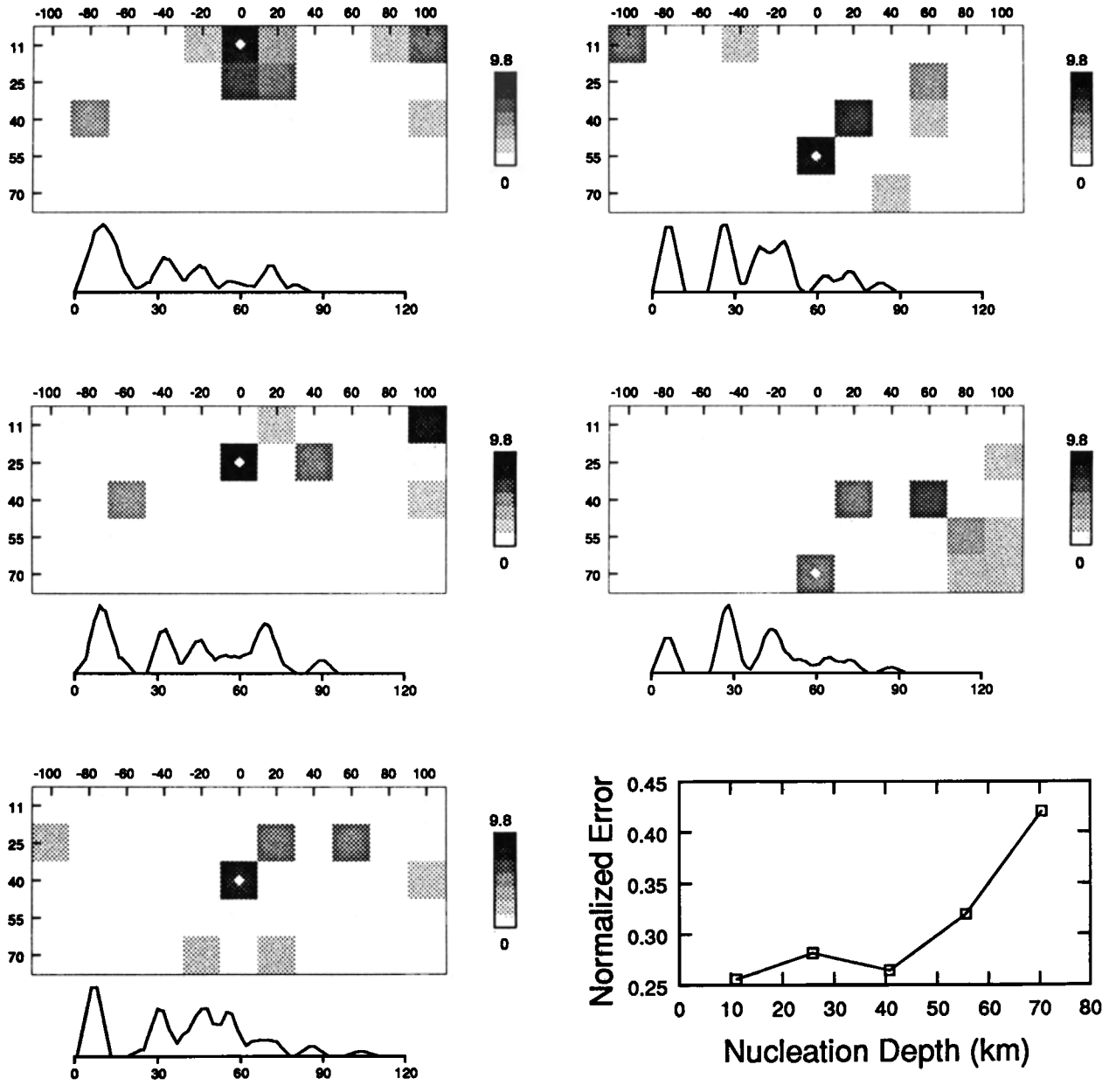

Fig. 10. Source functions and spatial plots of moment release (in 10^{27} dyn cm) for two-dimensional simultaneous deconvolution shown for all five possible nucleation depths, as indicated by the white diamond. The horizontal scales are distance in kilometers along strike, and the vertical scales indicate depth in kilometers. In the lower left the normalized error of the models (seismogram mismatch) is shown as a function of the assumed nucleation depth.

and v_r is the rupture velocity. The updip and downdip edges of the fault produce a truncation that forms the back side of a triangular pulse. Rupture lengthwise along a rectangular fault area, on the other hand, produces a constant moment release of $\mu(2Wv_r)D$.

The Sumba event can be qualitatively simulated by a superposition of these two types of ruptures. In fact, the ratio of the half length of the aftershock area to the width of the fault zone is about 2–3, which is similar to the ratio of the lengths of the trapezoid and the triangle of the Sumba source functions, suggesting that a simple rupture at a constant velocity can explain the data. The major drawback with this model is that for a bilateral rupture with uniform displacement the height of the rectangle should be about 2/3 the height of the triangle (Figure 12), while for the Sumba source functions, the trapezoid is less than 1/3 the height of the triangle (e.g., Figure 7).

One fairly straightforward interpretation is that the displacement varies in combination with the area expansion rate; i.e., we postulate an epicentral region with high displacement (Figure 13). In fact, we can estimate the variation in displacement over the fault for this model by inferring the displacement in the high-displacement region (D_1) from the peak moment release rate ($\langle \dot{M} \rangle$), and the average displacement for the whole fault (D_0) from the static moment (M_0) and fault dimensions:

$$\langle \dot{M} \rangle \approx \mu \langle \dot{A} \rangle D_1$$

and

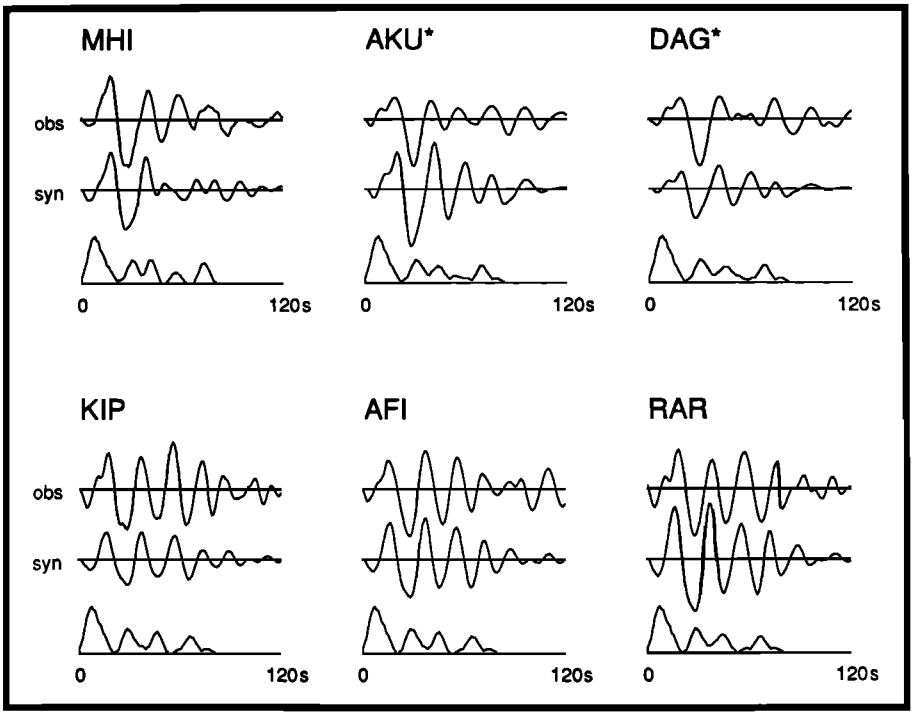

Fig. 11. Observed and synthetic seismograms for the first model in Figure 10 (nucleating at 11 km depth).

$$M_0 = \mu A_0 D_0$$

where $\langle \dot{A} \rangle$ is the rate at which the rupture area is expanding at the peak of the moment release function, and A_0 is the total area of the fault. For a circular rupture nucleating at the center of a rectangular fault with length L and width W,

$$A = LW$$

and

$$\langle \dot{A} \rangle = 2\pi v_r \frac{W}{2} = \pi \left[\frac{W}{2t_p}\right] W = \pi \frac{W^2}{2t_p}$$

where t_p is the time at which the rupture first reaches the edges of the fault. If the rupture nucleates at the updip or downdip edge and spreads semicircularly, $\langle \dot{A} \rangle$ is given by

$$\langle \dot{A} \rangle = \pi v_r W = \pi \left[\frac{W}{t_p}\right] W = \pi \frac{W^2}{t_p}$$

The fault width can be related to the depth extent, h, by $W=h/\sin\delta$, where δ is the dip of the fault.

The ratio of the average displacement in the central part (D_1) to that over the rest of the fault (D_2) can be obtained from the equation for the static moment:

$$\mu A_0 D_0 = \mu A_1 D_1 + \mu A_2 D_2$$

$$\frac{D_1}{D_2} = \frac{A_0 - A_1}{A_0(D_0/D_1) - A_1}$$

where A_1 is the area of the central part and is equal to $\pi W^2/4$ for a circular rupture and $\pi W^2/2$ for a semicircular rupture. The ratio D_1/D_2 is thus

$$\frac{D_1}{D_2} = \frac{4L - \pi W}{4L(D_0/D_1) - \pi W} \qquad \text{Circular}$$

$$\frac{D_1}{D_2} = \frac{2L - \pi W}{2L(D_0/D_1) - \pi W} \qquad \text{Semicircular}$$

For the 1977 Sumba earthquake we take the fault length (L) to be 200 km (a conservative estimate of the aftershock extent) and the fault dip (δ) to be 45°. (Note that increasing the fault length decreases the estimate of D_0, thus increasing the degree of displacement heterogeneity.) The average peak moment release rate ($\langle \dot{A} \rangle$) for the reliable undiffracted stations is 2.6×10^{27} dyn cm/s, and the average seismic moment (M_0) is 30×10^{27} dyn cm. The time of the peak moment release (t_p) is 14 s. In the theoretical plots of $\dot{A}$ (Figure 12), this time is equal to the duration time, since the rupture front changes instantaneously from radially propagating to horizontally propagating. We use the peak time in our calculations because if this change is not instantaneous, the apparent duration of the initial rupture will extend somewhat past t_p. However, the peak time will generally record the time at which the rupture front first interacts with the edges of the fault. The resulting displacements, displacement ratios, and rupture velocities for both the semicircular and circular rupture models are tabulated for several possible depth extents (Table 2).

All of the parameter combinations result in significant heterogeneity, except for the semicircular model with depth extents of 50 km or greater. However, these exceptions also require exceedingly high rupture velocities, suggesting that they are less reasonable models. Furthermore, they imply either a total fault length of almost 400 km (40 s × 5 km/s in each direction), which is unlikely, or a large decrease in rupture velocity after the initial rupture. The latter possibility would also be an indication of significant fault plane heterogeneity.

DISCUSSION

Since the origin of intraplate stresses, the process of stress accumulation, and even the existence of faults before the

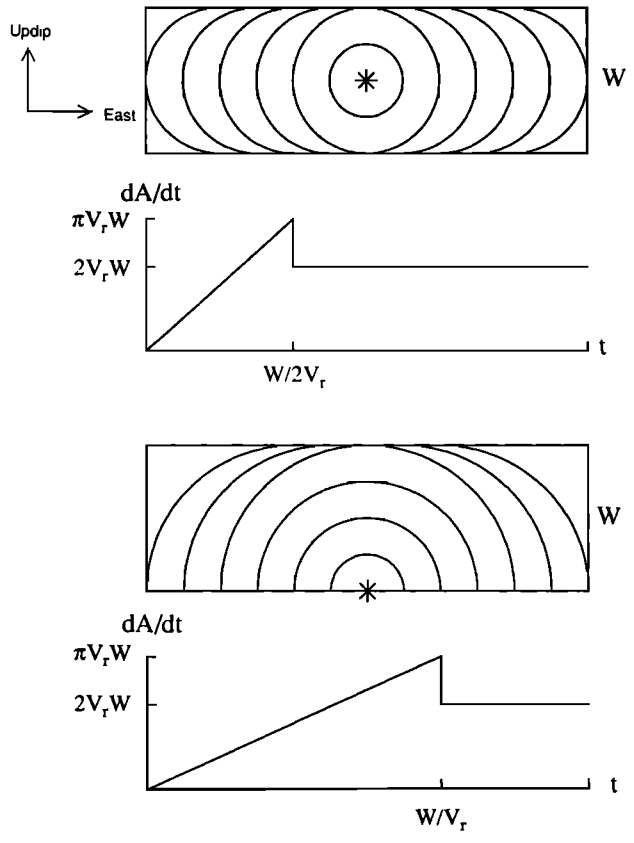

Fig. 12. Schematic diagram of rupture on a homogeneous fault, nucleating at the center of the fault (top) and at the downdip edge of the fault (bottom). Below each diagram is a plot of the area expansion rate, $\dot{A}$, as a function of time. (The source-time function, $\dot{M}$, can be obtained by multiplying $\dot{A}$ by μD.)

occurrence of major intraplate earthquakes are unknown, it is difficult to identify "asperities" (which represent high-failure-stress regions) on the Sumba fault. However, several characteristics of the rupture process of the 1977 Sumba earthquake are reminiscent of asperity rupture as documented for interplate earthquakes. The most important such feature is the significant variation in coseismic displacement, which implies spatial variations in static stress drop. Another such feature is the manner in which the rupture nucleated, beginning some 30–40 km away from the center of the high-displacement region, or in other words, near the periphery of this region. The rupture apparently also began with a very low level of energy release. This behavior bears some resemblance to the scenarios suggested for asperity rupture by numerical experiments [*Das and Kostrov*, 1983], in which the rupture front proceeds around the circumference of a circular asperity before the interior fails. A similar behavior was inferred by *Schwartz and Ruff* [1985] for the 1969 Tokachi-Oki earthquake. The event had initial weak radiation nucleating at the eastern edge of an inferred asperity, and the rupture front moved to the southern edge of the asperity before the asperity itself ruptured.

The relationship of the seismicity to the area of high displacement is also suggestive of an asperity. *Spence* [1986] shows that aftershock activity is sparse in the central portion of the rupture area, corresponding to the high-displacement, high-stress-drop region, and concentrated in the eastward lateral region along the trench (Figure 1), which we interpret as having less displacement. The latter region more likely represents a barrier, as it roughly coincides with the area where the Australian continental shelf is apparently thwarting subduction (Figure 1). It is also interesting to note that the foreshock that occurred one hour before the main shock has almost the same epicenter as the main shock, placing it at the periphery of the high-displacement region. This points to this particular location as representing a transition from a high stress concentration to a lower stress concentration, as would occur at the edge of an asperity.

Heterogeneous coseismic displacement has generally been difficult to document for large intraplate earthquakes. *Beck and Ruff* [1988] studied the 1970 Peru normal-faulting earthquake using single-station deconvolutions and directivity analysis and found evidence for two pulses of moment release (located well away from the epicenter), which might indicate variations in displacement along the fault. However, they also inferred a change in focal mechanism from normal to thrust for the second pulse. This would imply that the two pulses of moment release take place on two separate faults, so that heterogeneity on a single fault cannot be inferred. On the other hand, the source history inferred from the *P* waves of the 1975 North Atlantic earthquake (M_w=7.8) is composed of only a single, short (14 s) pulse [*Lynnes and Ruff*, 1985*a*], suggesting the data are well matched by a small homogeneous fault. Many studies have utilized the multiple-station technique of *Kikuchi and Fukao* [1985] to study large intraplate earthquakes [*Fukao and Kikuchi*, 1987; *Welc and Lay*, 1987; *Christensen and Lay*, 1988], some of which have multiple pulses of moment release. However, the parameterization of the technique makes assessment of the spatial resolution difficult, since the algorithm locates moment release at each iteration only at a single grid point. Consequently, more work needs to be done to determine whether large and great intraplate earthquakes generally rupture faults with homogeneous or heterogeneous strength distributions.

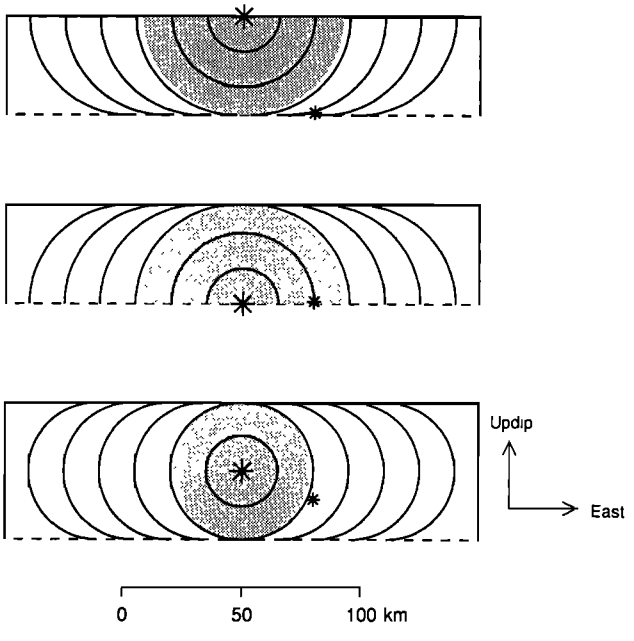

Fig. 13. Three possibilities for the rupture of the 1977 Sumba earthquake, with epicentral asperity (shaded region). The large asterisk shows the postulated focus of the main pulse, and the small asterisk marks the relative position of the precursor. The average displacement of the asperity and weak regions are shown below.

TABLE 2. Displacements and Rupture Velocities for Different Fault Models

Rupture Nucleation	Depth, km	Width, km	v_r, km/s	D_0, m	D_1, m	D_2, m	D_1/D_2
Semicircular	20	28	2.0	10.7	29.4	8.2	3.6
	30	42	3.0	7.1	13.0	5.9	2.2
	40	58	4.0	5.2	7.2	4.5	1.6
	50	71	5.1	4.2	4.6	3.8	1.2
Circular	20	28	1.0	10.7	58.8	7.7	7.6
	30	42	1.5	7.1	26.0	5.3	4.9
	40	58	2.0	5.2	14.4	4.0	3.6
	50	71	2.5	4.2	9.2	3.3	2.8

Although this study has failed to completely resolve the depth extent of the 1977 Sumba event, we have presented evidence in support of a relatively shallow (≤ 50 km) rupture extent. This might appear to support an earthquake due to bending stresses and to reaffirm the importance of bending in the flexure of the outer rise. However, even if the seismic rupture extended to only 30 km depth, it is still possible that the rest of the lithosphere (presumably more ductile) detached in such a way as to radiate predominantly very-long-period waves, such as a "slow" or "silent" earthquake, or even detached aseismically. There is some suggestion that such slip may have occurred, in that the *P* wave estimates of seismic moment, source duration and depth extent are less than some surface wave estimates, a discrepancy that could be explained by "slow" slip on a deeper extension of the fault. This might be similar to the discrepancy for the June 22, 1977 Tonga earthquake, for which a smaller vertical extent has been inferred from *P* wave deconvolutions [*Christensen and Lay*, 1988] than from long-period surface waves [*Lundgren and Okal*, 1988]. In the case of the 1977 Sumba earthquake, however, there are also surface wave and normal mode estimates of seismic moment, source duration and depth that do not conflict with the *P* wave estimates.

Whatever the true depth extent of the Sumba earthquake, its location may be so unusual that its relevance to the bending model of *Hanks* [1979] is questionable. As noted earlier, this area is devoid of major underthrusting earthquakes, and the ocean floor is quite old, both of which suggest an uncoupled subduction zone. This uncoupled nature is also implied by the occurrence of two outer-rise events (March 30, 1967 and May 28, 1972) to the west of the 1977 event, both with normal mechanisms [*Fitch*, 1972; *Cardwell and Isacks*, 1978]; *Christensen and Ruff* [1983] infer such events to be an indication of an uncoupled zone. In contrast, the Java trench is truncated directly to the east of the 1977 Sumba aftershock area by the subduction of continental crust (Australia). In fact, the aftershock area terminates here in a cluster of aftershocks highly suggestive of a lateral stress barrier of some type (Figure 1). The juxtaposition of old ocean crust and continental crust in the subduction zone provides one of the most dramatic lateral gradients in interplate seismic coupling in the world. The combination of slab pull on an uncoupled slab in the Java trench and the strong resistive force of the buoyant crust to the east apparently conspired to store a tremendous amount of elastic tensile strain energy in the lithosphere at the junction of the two zones [*Spence*, 1986], leading to the great Sumba earthquake.

CONCLUSIONS

Analysis of the long-period *P* waves from the 1977 Sumba earthquake indicates that the area ruptured during the event extended to about 30–50 km depth. From *pP* arrivals in the initial low-amplitude waveforms we conclude that the rupture nucleated at a depth of 29 km, and 30 km is also the greatest depth recorded for the aftershocks [*Dziewonski et al.*, 1981; *Fitch et al.*, 1981; *Spence*, 1986]. However, we are unable to rule out the possibility of additional moment release beneath 30–50 km, provided only very low frequencies are radiated, such as might be expected for a smooth rupture mode with a long source process time.

Deconvolutions of the *P* waves indicate a simple source history, consisting of a steep triangle on top of a low trapezoid with some minor high-frequency pulses superimposed. As there are no systematic azimuthal variations attributable to directivity, a bilateral rupture is inferred, although the *P* waves do not constrain the length. The data can be fit by a simple model consisting of bilateral rupture along a 200 km long fault, which is also consistent with the aftershock extent and the surface wave results of *Zhang and Kanamori* [1988]. However, calculations of the average displacement corresponding to the triangular part of the source function and to the fault as a whole imply a central region with displacements higher than those for the rest of the fault. This heterogeneity and the initial low-energy-release nucleation of the rupture at the edge of the central region are suggestive of an asperity, indicating that some analogue to the asperity model may be applicable to great intraplate earthquakes.

Acknowledgments. We thank Hiroo Kanamori, Jiajun Zhang, and Paul Silver for discussions on their techniques. We also thank Larry Ruff, Paul Lundgren, and two anonymous reviewers for many useful suggestions and for critically reading the manuscript. This research was supported by NSF grant EAR-8451715. Acknowledgment is made to the Donors of the Petroleum Research Fund administered by the American Chemical Society for the partial support of this research.

REFERENCES

Beck, S. L., and L. J. Ruff, The rupture process of the great 1979 Colombia earthquake: Evidence for the asperity model, *J. Geophys. Res.*, *89*, 9281–9291, 1984.

Beck, S. L., and L. J. Ruff, The rupture process of the 1976 Mindanao earthquake, *J. Geophys. Res.*, *90*, 6773–6782, 1985.

Beck, S. L., and L. J. Ruff, Rupture process of the great 1963 Kurile Islands earthquake sequence: Asperity interaction and multiple event rupture, *J. Geophys. Res.*, *92*, 14123–14138, 1987.

Beck, S. L., and L. J. Ruff, Great earthquakes and subduction along the Peru trench, *Phys. Earth Planet. Inter.*, in press, 1988.

Cardwell, R. K., and B. L. Isacks, Geometry of the subducted lithosphere beneath the Banda Sea in Eastern Indonesia from seismicity and fault plane solutions, *J. Geophys. Res.*, *83*, 2825–2838, 1978.

Christensen, D. H., and T. Lay, Large earthquakes in the Tonga region associated with subduction of the Louisville Ridge, *J. Geophys. Res.*, *93*, in press, 1988.

Christensen, D. H., and L. J. Ruff, Outer-rise earthquakes and seismic coupling, *Geophys. Res. Lett.*, *10*, 697–700, 1983.

Christensen, D. H., and L. J. Ruff, Analysis of the trade-off between hypocentral depth and source time function, *Bull. Seismol. Soc. Am.*, *75*, 1637–1656, 1985.

Das, S., and B. V. Kostrov, Breaking of a single asperity: Rupture process and seismic radiation, *J. Geophys. Res.*, *88*, 4277–4288, 1983.

Dziewonski, A. M., T.-A. Chou, and J. H. Woodhouse, Determination of earthquake source parameters from waveform data for studies of global and regional seismicity, *J. Geophys. Res.*, *86*, 2825–2852, 1981.

Fitch, T. J., Plate convergence, transcurrent faults, and internal deformation adjacent to Southeast Asia and the western Pacific, *J. Geophys. Res.*, *77*, 4432–4460, 1972.

Fitch, T. J., R. G. North, and M. W. Shields, Focal depths and moment tensor representations of shallow earthquakes associated with the great Sumba earthquake, *J. Geophys. Res.*, *86*, 9357–9374, 1981.

Fukao, Y., and M. Kikuchi, Source retrieval for mantle earthquakes by iterative deconvolution of long-period *P*-waves, *Tectonophysics, 144*, 249–269, 1987.

Furumoto, M., and I. Nakanishi, Source times and scaling relations of large earthquakes, *J. Geophys. Res., 88*, 2191–2198, 1983.

Giardini, D., A. M. Dziewonski, and J. H. Woodhouse, Centroid-moment tensor solutions for 113 large earthquakes in 1977-1980, *Phys. Earth Planet. Inter., 40*, 259–272, 1985.

Given, J. W., and H. Kanamori, The depth extent of the 1977 Sumbawa, Indonesia earthquake (abstract), *Eos Trans. AGU, 61*, 1044, 1980.

Hamilton, W., Tectonics of the Indonesian region, *U. S. Geol. Surv. Prof. Pap., 1078*, 1979.

Hanks, T. C., Deviatoric stresses and earthquake occurrence at the outer rise, *J. Geophys. Res., 84*, 2343–2347, 1979.

Hartzell, S. H., and T. H. Heaton, Teleseismic time functions for large, shallow subduction zone earthquakes, *Bull. Seismol. Soc. Am., 75*, 965–1004, 1985.

Kanamori, H., Seismological evidence for a lithospheric normal faulting—the Sanriku earthquake of 1933, *Phys. Earth Planet. Inter., 4*, 289–300, 1971.

Kanamori, H., and G. S. Stewart, Mode of the strain release along the Gibbs fracture zone, Mid-Atlantic ridge, *Phys. Earth Planet. Inter., 11*, 312–332, 1976.

Kikuchi, M., and Y. Fukao, Iterative deconvolution of complex body waves from great earthquakes—the Tokachi-Oki earthquake of 1968, *Phys. Earth Planet. Inter., 37*, 235–248, 1985.

Kikuchi, M., and Y. Fukao, Inversion of long-period *P*-waves from great earthquakes along subduction zones, *Tectonophysics, 144*, 231–247, 1987.

Kikuchi, M., and H. Kanamori, Inversion of complex body waves, *Bull. Seismol. Soc. Am., 72*, 491–506, 1982.

Lerner-Lam, A. L., and T. H. Jordan, How thick are the continents?, *J. Geophys. Res., 92*, 14007–14026, 1987.

Lundgren, P., and E. Okal, Slab decoupling in the Tonga arc: The June 22, 1977 earthquake, *J. Geophys. Res., 93*, in press, 1988.

Lynnes, C. S., and L. J. Ruff, Source process and tectonic implications of the great 1975 North Atlantic earthquake, *Geophys. J. R. Astron. Soc., 82*, 497–510, 1985*a*.

Lynnes, C. S., and L. J. Ruff, Use of the *PP* phase to study the earthquake source, *Geophys. Res. Lett., 12*, 514–517, 1985*b*.

Madariaga, R., High frequency radiation from dynamic earthquake fault models, *Ann. Geophys., 1*, 17–23, 1983.

Ruff, L. J., and H. Kanamori, The rupture process and asperity distribution of three great earthquakes from long-period diffracted *P*-waves, *Phys. Earth Planet. Inter., 31*, 202–230, 1983*a*.

Ruff, L. J., and H. Kanamori, Seismic coupling and uncoupling at subduction zones, *Tectonophysics, 99*, 99–117, 1983*b*.

Savage, J. C., Relation of corner frequency to fault dimensions, *J. Geophys. Res., 77*, 3788–3795, 1972.

Schwartz, S. Y., and L. J. Ruff, The 1968 Tokachi-Oki and the 1969 Kurile Islands earthquakes: Variability in the rupture process, *J. Geophys. Res., 90*, 8613–8626, 1985.

Silver, P. G., and T. H. Jordan, Total-moment spectra of fourteen large earthquakes, *J. Geophys. Res., 88*, 3273–3292, 1983.

Silver, P. G., M. A. Riedesel, T. H. Jordan, and A. F. Sheehan, Low frequency properties of the Sumbawa earthquake of 1977 (abstract), *Eos Trans. AGU, 67*, 309, 1986.

Spence, W., The 1977 Sumba earthquake series: Evidence for slab pull force acting at a subduction zone, *J. Geophys. Res., 91*, 7225–7239, 1986.

Stewart, G. S., Implications for plate tectonics of the August 19, 1977 Indonesian decoupling normal fault earthquake, (abstract) *Eos Trans. AGU, 59*, 326, 1978.

Strehlau, J., A discussion of the depth extent of rupture in large continental earthquakes, in *Earthquake Source Mechanics, Maurice Ewing Ser.*, vol. 6, edited by S. Das, J. Boatwright, and C. H. Scholz, p. 131 AGU, Washington, D. C., 1986.

Welc, J. L., and T. Lay, The source rupture process of the Great Banda Sea earthquake of November 4, 1963, *Phys. Earth Planet. Inter., 45*, 242–254, 1987.

Zhang, J., and H. Kanamori, Determination of vertical extent of faulting of large earthquakes using long-period surface waves (abstract), *Eos Trans. AGU, 66*, 963, 1985.

Zhang, J., and H. Kanamori, Source finiteness of large earthquakes measured from long-period Rayleigh waves, *Phys. Earth Planet. Inter.*, in press, 1988.

T. Lay, Dept. of Geological Sciences, University of Michigan, Ann Arbor, MI 48109.

C. S. Lynnes, Teledyne Geotech, 314 Montgomery Street, Alexandria, VA 22314.

(Received November 20, 1987;
revised May 5, 1988;
accepted July 8, 1988.)